Alexandria Engineering Journal (2022) 61, 1217–1234

HOSTED BY

Alexandria University

Alexandria Engineering Journal

www.elsevier.com/locate/aej
www.sciencedirect.com

Role of fluid-structure interaction in free convection in square open cavity with double flexible oscillating fins

Habibis Saleh [a], Kohilavani Naganthran [b], Ishak Hashim [b,*], Mohammad Ghalambaz [c,d], Roslinda Nazar [b]

[a] Mathematics Education Department, Universitas Islam Negeri Sultan Syarif Kasim Riau, 28293 Pekanbaru, Indonesia
[b] Department of Mathematical Sciences, Faculty of Science & Technology, Universiti Kebangsaan Malaysia, 43600 UKM Bangi Selangor, Malaysia
[c] Metamaterials for Mechanical, Biomechanical and Multiphysical Applications Research Group, Ton Duc Thang University, Ho Chi Minh City, Vietnam
[d] Faculty of Applied Sciences, Ton Duc Thang University, Ho Chi Minh City, Vietnam

Received 29 January 2020; revised 5 January 2021; accepted 24 April 2021
Available online 22 August 2021

KEYWORDS

Free convection;
FEM;
Arbitrary Lagrangian–Eulerian;
Open boundary;
Flexible fin;
FSI

Abstract The problem of transient free convection in an open cavity containing two elastic thin fins is studied in this paper. The left surface is heated, and the right surface is in opening, which is in contact with the environment air. The dimensionless forms of the governing equations for continuity, momentum and heat transfer in the fluid and structures domains are written in Arbitrary Lagrangian–Eulerian (ALE) formulation. The governing equations are solved by the finite element method (FEM). The governing parameters considered are the oscillating fin direction, fin amplitude and length with several flexibility values and aperture sizes. The results show that a maximum heat transfer enhancement occurs at the suitable parameters between the aperture size and the fins oscillating direction.

1. Introduction

Most of the emphasis today in the thermal engineering studies are devoted to extending forced convection to dissipate the heat. However, in practical situations still be subject to free convection strategy on removing the heat. Basically, free convection strategy combined with enclosure configuration is what results when an external help is not used in the device design to move air. Instead, movement of the air is brought by density

* Corresponding author.
E-mail addresses: Dr.habibissaleh@gmail.com (H. Saleh), kohi@ukm.edu.my (K. Naganthran), ishak_h@ukm.edu.my (I. Hashim), mohammad.ghalambaz@tdtu.edu.vn (M. Ghalambaz), rmn@ukm.edu.my (R. Nazar).

Peer review under responsibility of Faculty of Engineering, Alexandria University.

https://doi.org/10.1016/j.aej.2021.04.073
1110-0168

Nomenclature

Roman letters

A^*	oscillation amplitude [m]
b^*	elastic fin thickness [m]
Cp_f	specific heat capacity of the fluid [J/kg K]
Cp_s	solid specific heat capacity [J/kg K]
$\mathbf{d}_s^*$	displacement vector [m]
E^*	Young's modulus [N/m]
$\mathbf{F}_v^*$	body force [N/m^3]
$\mathbf{g}$	gravity [m/s^2]
H^*	aperture size [m]
k_f	thermal conductivity of the fluid [W/m K]
k_s	solid thermal conductivity [W/m K]
ℓ	square enclosure width [m]
L^*	elastic fin length [m]
Nu	instantaneous local Nusselt number [–]
$\overline{Nu}$	average Nusselt number [-]
$\overline{Nu}(t)$	transient averaged heat transfer [-]
$\overline{\overline{Nu}}$	average Nusselt number over time [-]
p^*	fluid pressure [Pa]
Pr	Prandtl Number [-]
Ra	Rayleigh Number [-]
$\mathbf{S}$	second Piola–Kirchhoff stress tensor [Pa]
T	temperature [K]
T_h	left wall temperature [K]
T_∞	ambient temperature [K]
t^*	time [s]
t_p^*	oscillation period [s]
$\mathbf{u}^*$	fluid velocity [m/s]
u, v	velocityx, y-direction [m/s]
$\mathbf{w}^*$	changing position velocity [m/s]
x^*, y^*	space ordinate [m]

Greek symbols

α_f	thermal diffusivity of the fluid [m^2/s]
α_s	thermal diffusivity of the solid [m^2/s]
β	coefficient of thermal expansion [1/K]
ε	strain [-]
ν_f	viscosity [Pa s]
ρ_f	fluid density [kg/m^3]
ρ_s	density of the fin [kg/m^3]
σ^*	stress tensor [Pa]
ψ^*	stream function [-]

differences coming from the thermal dissipation by the heated components. A distinct advantage of free convection is that the expense of incorporating the external help is avoided. Of course the penalty associated with this strategy is lower heat transfer rate. The recent heat transfer and fluid dynamics application are nanofluids, suspending nanoparticles in the host fluid. Flowing nanofluids in contact with a surface were shown by Gupta et al. [1], Gupta et al. [2] and Gupta et al. [3] effective to increase the heat transfer rate.

Heat transfer within cavities are encounter in thermal management solar panels, cavities filled with gas around the cores of nuclear reactors, cooling of electronic components, thermal insulation and fuel cells. Valuable works of by Ostrach [4] have contributed to the early development of the mathematical modelling for free convection studies in enclosed cavities. de Vahl Davis [5] have proposed the bench mark numerical solution and after that numerous works which investigate the free convection in this configuration from various perspective have been reported. Ostrach [6] made a critical review of free convection problems in several cavity shapes and configurations from the aspect of experimental and theoretical approaches. Different cavity configuration such a side opening where the ambient air from outside cavity facilitate the cooling of the internal components were studied by Penot [7] and Chan and Tien [8]. The effect of the opening on the induced flow in terms of the size and the location of the opening was investigated by Abib and Jaluria [9]. Angirasa et al. [10] and Angirasa et al. [11] studied the unsteady heat transfer in a square open cavity. Chakroun et al. [12], Elsayed et al. [13] and Bilgen and Oztop [14] considered an open tilted cavity. Lauriat and Desrayaud [15] included the effect of surface radiation on conjugate natural convection in partially open cavity. Kasayapanand [16] examined the problem of electrohydrodynamics on natural convection in partially open cavity and his extended work [17]. He found the volume flow rate and heat transfer enhancement were significantly improved at the low aperture size and high aperture position and the flow rate and the enhancement reached to a maximum point at the extreme electrode configuration for multiple fins. Mahmoudi et al. [18] obtained the flow and thermal distributions of the nanofluids inside the open cavity depends on the Rayleigh numbers and the location of the heat sources. Kefayati et al. [19] showed that the convective flow inside the open cavity increases with augmentation of Rayleigh number and the nanoparticles concentration. Recently, Wang et al. [20] found that the two openings on the same side strengthened the flow interaction between the cavities and then improve the heat transfer.

There is another class of problems which is designated as Fluid–Structure Interaction (FSI), and it focused on the mutual relationship between the fluid and structures or any additional advance material embedded in the cavity. This external help were reported by Sheu et al. [21] that got the maximal 64% heat transfer improvement with energy load 5 W only. They embedded the multiple oscillating piezoelectric fin at the wall. Soti et al. [22] demonstrated effective heat transfer improvement from increased mixing due to deformation of a thin flexible plate. Ali et al. [23] presented a technique of heat transfer enhancement using flexible flaps. The effect of a single deformable fin on heat transfer has been examined by Ghalambaz et al. [24] and Alsabery et al. [25]. Larger amplitude oscillation improves considerably the thermal performance. Saleh et al. [26] discussed the function of FSI on combined convection in an enclosed cavity which is embedded with a circular cylinder along with dual oscillating fins. They concluded that the strength of the convective flow is highly dependent on the manner of the fins oscillation. Mehryan et al. [27] studied the impact of a thin flexible heater plate to the convective structure in an enclosure. Later, Ghalambaz et al. [28]

extended to the different working fluid, i.e. non-Newtonian fluid. Recently, Jamesahar et al. [29] considered the working fluids are nanofluids, and two oscillating flexible fins were attached to the enclosure.

These works give a vision to the present study to probe the effect of two oscillating fins on the convection heat transfer efficiency with varying the aperture size. The applications of the open-ended cavity for example in configuring vent openings of the electronic device. The importance of this problem arises when assuming one of the cavity walls at constant high temperature. In this case, we can simulate and improve the process of cooling of electronic components, which is a crucial factor in developing of computers processors. The oscillating fins create flow circulations, when these inner vortices collide with ambient air particles, momentum is transferred between the two particles, and a continuous stream of air is produced and directed toward electronic systems in the device. Previous configuration for having two inlet and outlet small openings by Ismael and Jasim [30] found that the proximity of the fin to the inlet opening increased the thermal performance.

2. Mathematical Formulation

The mathematical formulation starts with a model diagram which is drawn in Fig. 1. The Cartesian coordinate of an open square cavity is included in the figure. The fluid is initially assumed quiescent. The square enclosure width is ℓ and the partially open right boundary has aperture size H^*. Two thin elastic fins are attached on the left wall which is heated at T_h. The fins are of equal thickness b^* and length L^*. The open part of right surface is in contact with the ambient air, $T = T_\infty$ ($T_\infty < T_h$), while the other boundaries are all insulated. The end of the upper elastic fin moves following the trigonometry function:

$$y^* = A^* \sin\left(\frac{2\pi t^*}{t_p^*}\right), \tag{1}$$

at the same time, the lower flexible fin moves following the trigonometry function:

$$y^* = \pm A^* \sin\left(\frac{2\pi t^*}{t_p^*}\right), \tag{2}$$

where y^* is the ordinate of the right side of the elastic fins. Both of the fins might be oscillated identical or contrary depending on the sign value of the function 2. The time is represented by t^*, A^* is the oscillation amplitude and the oscillation period is symbolized by t_p^*. Temperature variation between the hot and cold side brings to a natural convection problem. The dynamic structural position of the elastic fin is formulated in the form of second order differential equation included heat transfer equation, as follow:

$$\rho_s \frac{d^2\mathbf{d}_s^*}{dt^{*2}} = \mathbf{F}_v^* + \nabla\sigma^*, \tag{3}$$

$$\frac{\partial T^*}{\partial t^*} = \alpha_s \nabla^2 T^*, \tag{4}$$

where ρ_s and $\mathbf{d}_s^*$ denote respectively the fin's density and displacement vector. The body force, stress tensor, temperature and solid thermal diffusivity are represented by $\mathbf{F}_v^*, \sigma^*, T^*$ and $\alpha_s = k_s/(\rho_s C p_s)$, respectively.

In the Arbitrary Lagrangian–Eulerian (ALE) formulation, the governing equations can be written as [24]

$$\nabla \cdot \mathbf{u}^* = 0, \tag{5}$$

$$\frac{\partial \mathbf{u}^*}{\partial t^*} + (\mathbf{u}^* - \mathbf{w}^*) \cdot \nabla \mathbf{u}^* = -\frac{1}{\rho_f}\nabla p^* + \nu_f \nabla^2 \mathbf{u}^* + \beta \mathbf{g}(T^* - T_c), \tag{6}$$

$$\frac{\partial T^*}{\partial t^*} + (\mathbf{u}^* - \mathbf{w}^*) \cdot \nabla T^* = \alpha_f \nabla^2 T^*, \tag{7}$$

with the fluid velocity, changing position velocity and the relative velocity are denoted by $\mathbf{u}^*, \mathbf{w}^*$ and $(\mathbf{u}^* - \mathbf{w}^*)$ respectively. The fluid pressure, density, viscosity, thermal diffusivity are denoted by p^*, ρ_f, ν_f, and $\alpha_f = k_f/(\rho_f C p_f)$ respectively. The gravity and coefficient of thermal expansion are represented by $\mathbf{g} = (0, -g)$ and β.

The model via streamfunction for fluid circulation is

$$\frac{\partial v^*}{\partial y^*} - \frac{\partial u^*}{\partial x^*} = \nabla^2 \psi^*. \tag{8}$$

Taking the flexible fins having a hyper-elastic property and applying the Winslow model and considering the nonlinear geometry factor, the stress tensor σ^* is stated as

$$\sigma^* = \mathbf{J}^{-1}\mathbf{F}\mathbf{S}\mathbf{F}^T, \tag{9}$$

where $\mathbf{F} = (\mathbf{I} + \nabla \mathbf{d}_s^*), \mathbf{J} = |\mathbf{F}|, \mathbf{S} = \mathbf{C} : (\varepsilon)$ with $\varepsilon = (\nabla \mathbf{d}_s^* + \mathbf{d}_s^{*T} + \mathbf{d}_s^{*T} \nabla \mathbf{d}_s^*)/2$ and $\mathbf{C} = \mathbf{C}(\mathbf{E}^*, \nu)$. The operator $\mathbf{S}$ refers to the second Piola–Kirchhoff stress tensor with ε is the strains.

At the fluid–solid interface of the flexible part we have the continuity of kinematic forces and dynamic movements. Referring to the regular no-slip condition for the interface, then

$$\frac{D\mathbf{d}_s^*}{Dt^*} = \mathbf{u}^* \quad \text{and} \quad \sigma^* \cdot \mathbf{n} = -p^* + \mu_f \nabla \cdot \mathbf{u}^* \tag{10}$$

The interface condition for the energy balance is:

$$k_f \frac{\partial T^*}{\partial n} = k_s \frac{\partial T^*}{\partial n}, \tag{11}$$

where the subscripts f and s denote respectively the fluid domain and the solid-fin domain. The fins are fastened with $\partial d_s^*/\partial t^*$. We assume zero pressure constraint at the cavity's bottom left corner. Defining the following dimensionless quantities,

$$\begin{aligned}
&d_s = \frac{d_s^*}{L^*}, \sigma = \frac{\sigma^*}{E^*}, (x, y) = \frac{(x^*, y^*)}{L^*}, (A, L, b) = \frac{(A^*, L^*, b^*)}{\ell}, \\
&t = \frac{t^* \alpha_f}{\ell^2}, \mathbf{u} = \frac{\ell \mathbf{u}^*}{\alpha_f}, \mathbf{w} = \frac{\ell \mathbf{w}^*}{\alpha_f}, p = \frac{p^* \ell^2}{\rho_f \alpha_f^2}, T = \frac{T^* - T_c}{T_h^* - T_c}, \\
&Ra = \frac{g\beta T_h^* - T_c \ell^3}{\nu_f \alpha_f}, \\
&Pr = \frac{\nu_f}{\alpha_f}, \\
&H = \frac{H^*}{\ell}, \\
&\alpha_r = \frac{\alpha_f}{\alpha_s}, \\
&k_r = \frac{k_f}{k_s},
\end{aligned} \tag{12, 13}$$

the flexible dynamic solid displacement, the fin heat transfer, continuity, momentum and heat transfer equation can be stated as [24]:

(a)

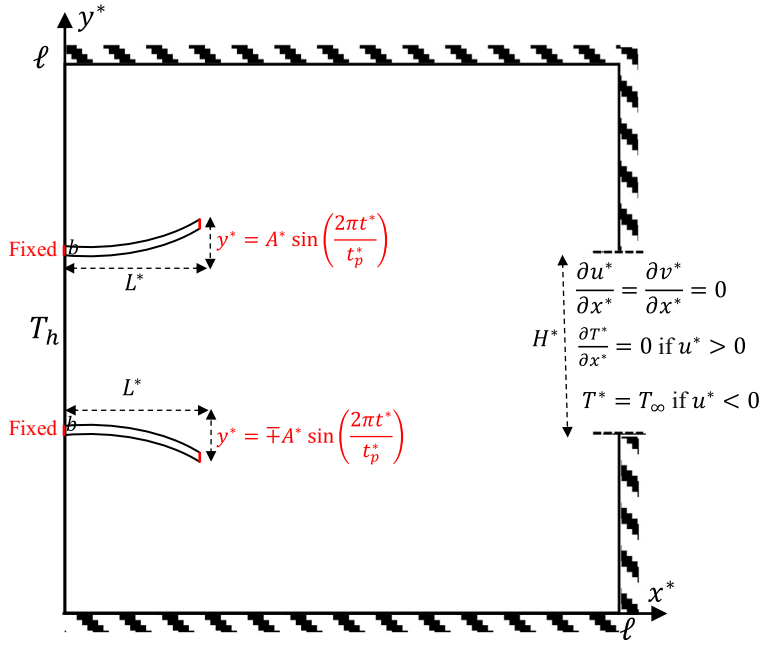

(b)

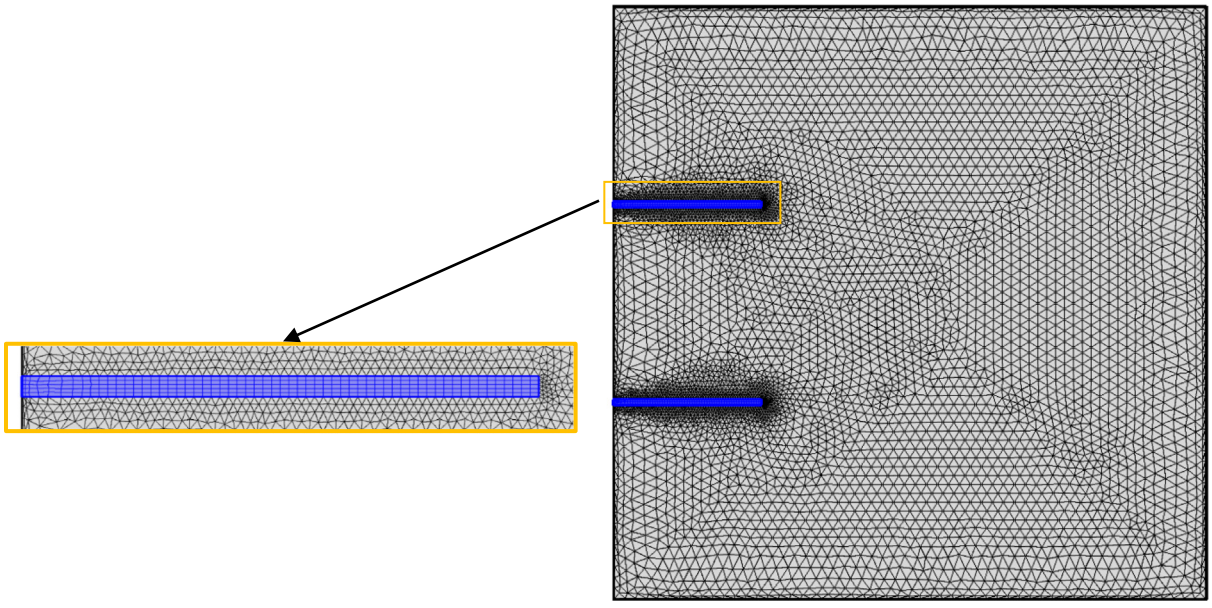

Fig. 1 (a) Schematic model of the square open cavity, (b) Mesh distribution.

$$\frac{1}{\rho_r}\frac{d^2 d_s}{dt^2} - E\nabla\sigma = EF_v, \tag{14}$$

$$\frac{\partial T}{\partial t} = \alpha_r \nabla^2 T, \tag{15}$$

$$\nabla \cdot \mathbf{u} = 0, \tag{16}$$

$$\frac{\partial \mathbf{u}}{\partial t} + (\mathbf{u} - \mathbf{w}) \cdot \nabla \mathbf{u} = -\nabla p + Pr\nabla^2 \mathbf{u} + Pr\,Ra\,T, \tag{17}$$

$$\frac{\partial T}{\partial t} + (\mathbf{u} - \mathbf{w}) \cdot \nabla T = \nabla^2 T. \tag{18}$$

The dimensionless streamfunction can be stated as

$$\frac{\partial^2 \psi}{\partial x^2} + \frac{\partial^2 \psi}{\partial x^2} = \frac{\partial u}{\partial y} - \frac{\partial v}{\partial x}. \tag{19}$$

The dimensionless initial and boundary conditions are [14]

$$u = 0,\ T = 0.5 \text{ at the fluid and solid domain,} \tag{20}$$

$u = 0,\ T = 1$ at the left surface,

$T = 0$ if $u < 0$,

$\frac{\partial T}{\partial x} = 0$ if $u > 0$,

$$-p + \mathrm{Pr}\nabla \cdot \mathbf{u} = 0 \text{ at the opening surface,} \tag{21}$$

$$\frac{\partial T}{\partial n} = k_r \frac{\partial T}{\partial n} \text{ for the fin.} \tag{22}$$

The no-slip condition at the fluid–solid is

$$\frac{D\mathbf{d}_s}{Dt} = \mathbf{u} \quad \text{and} \quad E\sigma \cdot \mathbf{n} = -p + \mathrm{Pr}\nabla \cdot \mathbf{u}. \tag{23}$$

The dimensionless pressure constraint is stated as:

$$p = 0 \tag{24}$$

at the corner of the cavity. The upper and lower fins movements are respectively given by

$$y = A \sin\left(\frac{2\pi t}{tp}\right), \tag{25}$$

$$y = \pm A \sin\left(\frac{2\pi t}{tp}\right). \tag{26}$$

The local Nusselt number along $x = 0$ is

$$Nu = \frac{h \cdot y}{k_f}, \tag{27}$$

where h is the convective heat transfer coefficient at $x = 0$. The instantaneous non-dimensional local Nusselt number evaluated at the hot wall can be divided into two parts:

$$Nu_f(t) = -\frac{\partial T(t)}{\partial x} \text{ at the fluid surface,} \tag{28}$$

$$Nu_s(t) = -k_r \frac{\partial T(t)}{\partial x} \text{ at the fin basis.} \tag{29}$$

The transient averaged heat transfer at the hot surface is defined by

$$\overline{Nu}(t) = \int_0^{\frac{1-b}{2}} Nu_f(t)\mathrm{d}y + \int_{\frac{1-b}{2}}^{\frac{1+b}{2}} Nu_s(t)\mathrm{d}y + \int_{\frac{1+b}{2}}^{1} Nu_f(t)\mathrm{d}y. \tag{30}$$

The average Nusselt number over time can be calculated as:

$$\overline{\overline{Nu}} = \int_1^{1+2t_p} \overline{Nu}(t)\mathrm{d}t. \tag{31}$$

The oscillating flexible fins achieved to a semi-steady state at $t \approx 1$. Two repeated sequence from the steady state $(1 + 2t_p)$ were commenced to maintain a stable result.

3. Solution approach

The dimensionless governing equations together with the boundary conditions are transformed into the weak form. Due to the oscillations of the fins in a fluid, it is more efficient to utilize a moving grid system. We use the Arbitrary Lagrangian–Eulerian (ALE) method to approximate the governing equations in moving and fixed boundary domains. The Galerkin finite element method are employed to discretize the nonlinear weak form of the equations. The Galerkin finite element method is preferable because complex geometries and irregular shapes modeling are easier as varieties of finite elements are available for the domain's discretisation. Moreover, in the Galerkin finite element method, boundary conditions can be easily incorporated, and different types of material properties can be easily accommodated in modeling from element to element or even within an element. However, the Galerkin finite element method requires a longer execution time, and involves a large amount of data as input for the mesh used in terms of nodal connectivity and other parameters depending on the problem.

Next, proper selection of an adequate time step is important in phase change heat transfer. Initially, the time step is set to 4.7×10^{-11}, then later adjusting time step following the period is performed, $t_p/40$. An implicit time step method based on the Backward Differentiation Formula (BDF) independent of time step is employed [31]. The minimum order of BDF is set at 2, while setup the maximum order is 1. To obtain good accuracy and convergence, the BDF solver estimates the value between the accuracy of the existing time steps, and then automatically sets the acceptable calculation time step [25]. The continuity, momentum, heat equations, flexible structure, and the grid movement are solved segregatedly until the convergence in the time step is reached.

The closed-form solution is achieved if the errors are below 10^{-6}. The calculations are then repeated until t ends. The convergence plot presents the reciprocal of the time step size, as shown in Fig. 2 (a). The reciprocal over the time step size. The greater the steps, the lower the value. The oscillation time step greater than 500 happens due to automatic time stepping and cyclic type of time-dependent tip motion. Time-dependent solver above has the adaptability to fit the time step size. The solver adjusts the step size that implies it reaching the converge. Fig. 2 (b) shows the relative residual for each time step size. This plot indicates that there are very small residuals so that the solutions are accepted. (see Table 1).

Several grid sensitivity evaluations were conducted as done in Saleh et al. [26]. Based on the CPU time, the extra fine grid was chosen in this study. As a verification, our computed values of the average Nusselt number agree well with that of Hinojosa et al. [32] and Chan and Tien [8] for the case of no fins installed when $Pr = 1$ as displayed in Table 2. Another validation is done in Fig. 3 against the work of Ghalambaz et al. [24] for free convection in a cavity with a single flexible fin installed

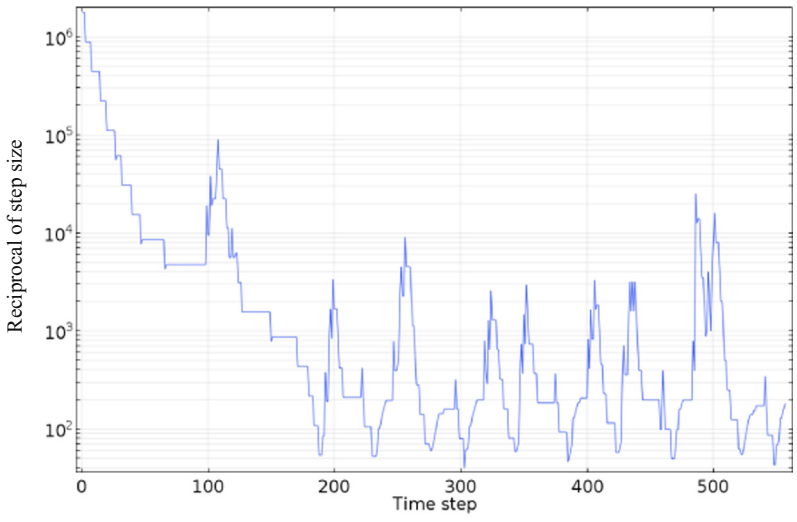

(a)

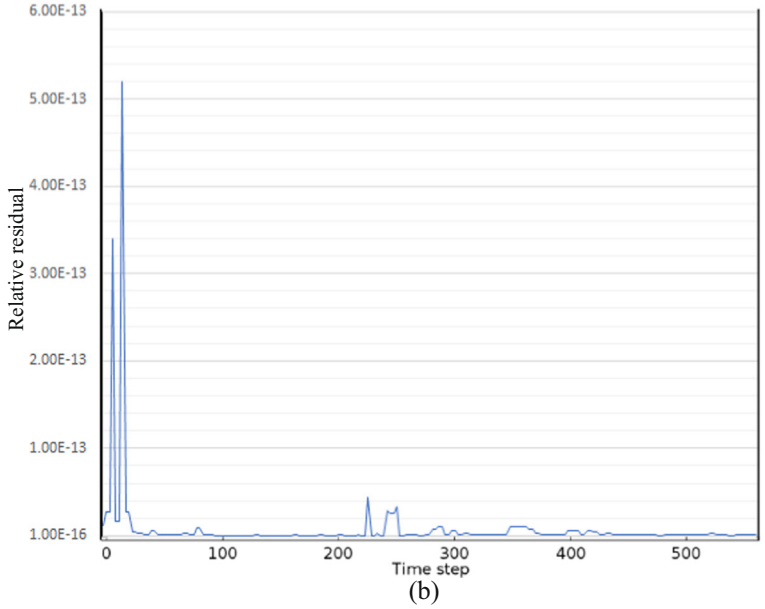

(b)

Fig. 2 The reciprocal and relative residual of the time step size at $L = 0.25, E = 10^9, A = 0.1, H = 0.5, Ra = 10^6$ and $t_p = 0.5$.

Table 1 Grid sensitivity checks at point $(x = 0.4, y = 0.8)$ for the fins oscillating in the same direction, $E = 10^9, A = 0.1, L = 0.25, H = 0.5$ and $t_p = 0.5$.

Predefined mesh size	Domain elements	Boundary elements	$T_{t=0.0125}$	$T_{t=1.125}$	CPU time (s)
Normal	3076	261	0.1011	0.4431	458
Fine	3772	293	0.1066	0.4474	763
Finer	5466	362	0.1144	0.4502	1047
Finer	4759	313	0.1175	0.4533	2393
Extra fine	11004	468	0.1204	0.4601	4776
Extremely fine	31624	770	0.1213	0.4609	18921

to the hot vertical wall for $t = 1.375, Ra = 10^6, A = 0.1, t_p = 0.5$ and $E = 10^{11}$. The two streamlines and isotherms shown in Fig. 3 compare reasonably well. Hence we are confident with the robustness and accuracy of the current method.

4. Results and discussion

This section intends to explain the outcome of the numerical simulation for the present model, which has been given in

Table 2 Comparison of the average Nusselt number results for the square open cavity with $Pr = 1$.

Ra	Present work	Hinojosa et al. [32]	Chan and Tien [8]
10^4	3.60	3.57	3.41
10^5	7.67	7.75	7.69
10^6	14.88	15.11	15.00
10^7	27.67	28.70	28.60

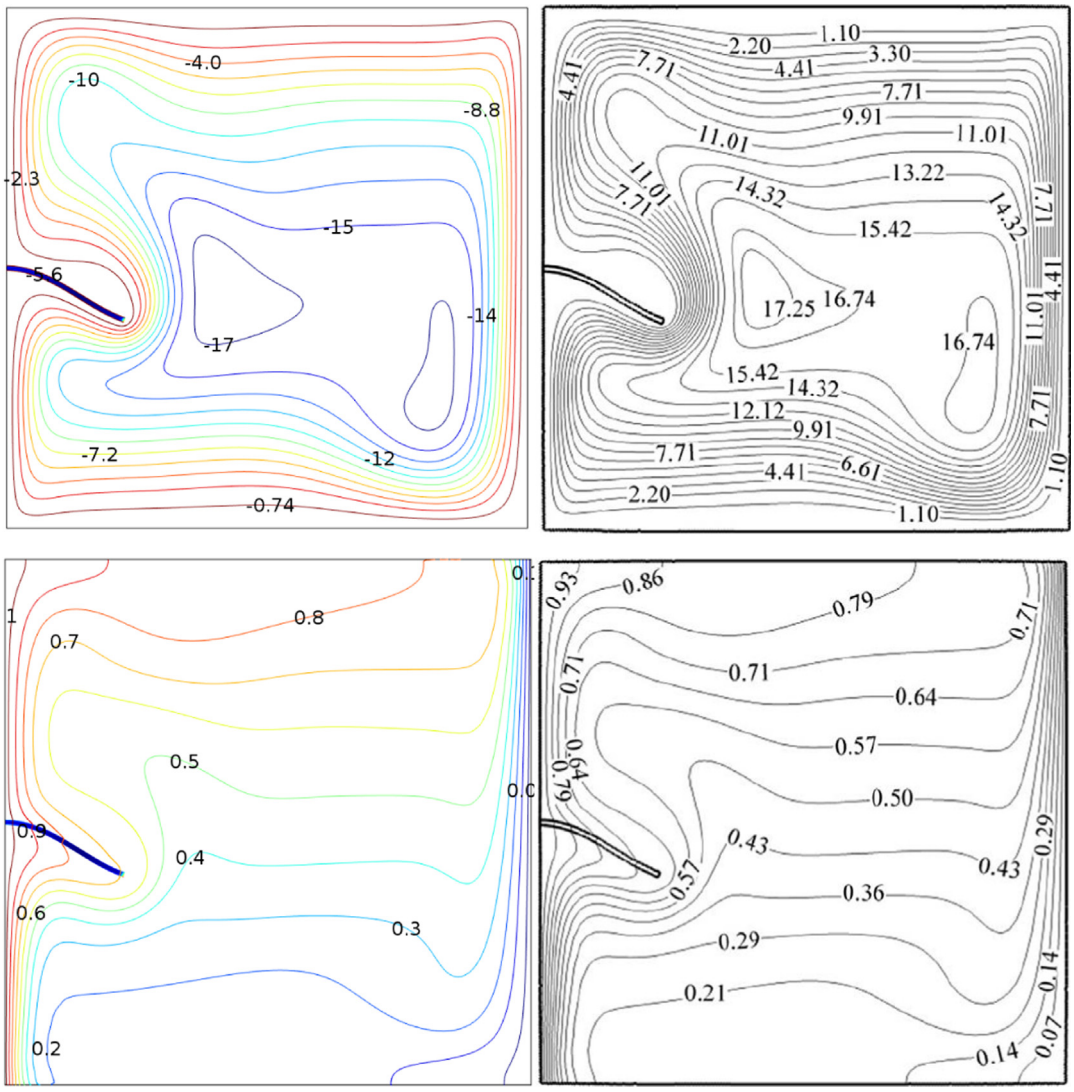

Fig. 3 Validation of computed streamlines and isotherms of the current work (left) with that of Ghalambaz et al. [24] (right) for the single fin at $t = 1.375, Ra = 10^6, A = 0.1, t_p = 0.5$ and $E = 10^{11}$.

(14)–(26). The physical interactions between the fluid and the structure (flexible fins) were conveyed through the logical manipulation of the governing parameters' values such as t (dimensionless time steps), Ra (the Rayleigh number), H (aperture size), E (Young's modulus), and A (amplitude of the oscillating fins) from the aspect of streamlines, isotherms, instantaneous Nusselt number, $Nu(t)$ and the average Nusselt number, $\overline{Nu}(t)$. The value of the Prandtl number fixed to be 0.71 and this portray air as the contacting medium. Mass and heat fluxes are zero at the right wall opening, and hence there is no interaction between the fluid within the cavity and the fluid outside of the cavity. Meshing is a crucial step in solving any computational fluid dynamics problems as it eases the computational process which obeys the Finite Element Method (FEM). Fig. 4 captures several snapshots of the moving mesh surrounding the two oscillating fins during

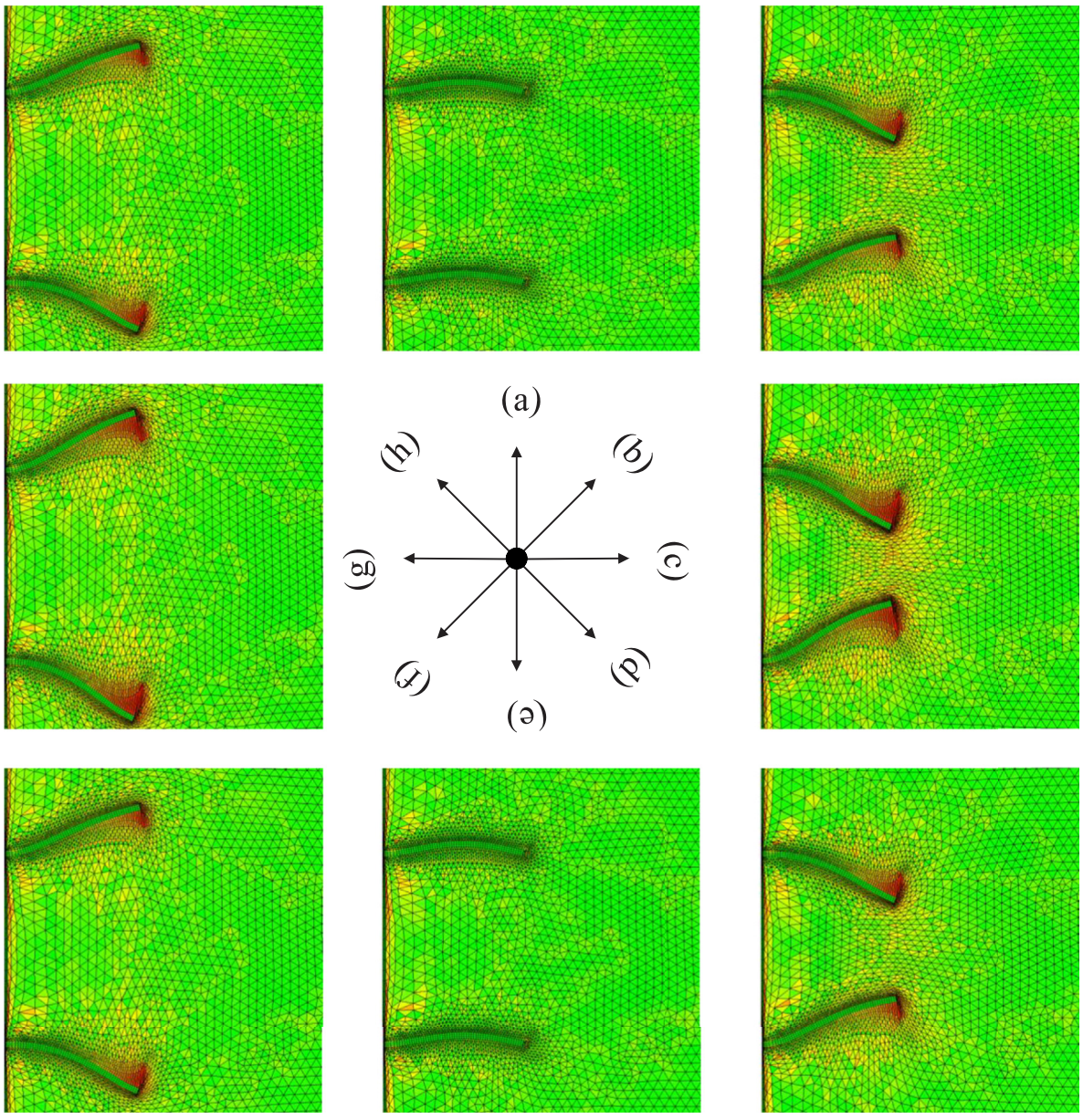

Fig. 4 A photograph of the moving mesh surrounding the double oscillating fins during one cycle from $t = 1.0$ and two oscillation when $E = 10^9, A = 0.1, H = 0.5$ and $t_p = 0.5$.

one cycle of oscillation after a semi-steady condition has been attained at $E = 10^9, A = 0.1, H = 0.5$ and $t_p = 0.5$. The higher density meshes are apparent near the oscillating fins so that accurate numerical results could be generated. The subplot pairs of (a)&(e), (b)&(d), and (h)&(f) show the symmetrical mesh because the movement of the upper and lower fins are based on the prescribed displacement as defined in Eqs. (24) and (25), respectively. Since the oscillation pattern is the same for each fin, all consecutive subplots are similar for the respective fins position.

Fig. 5 describes the chronology of the streamlines and velocity vectors for two identical flexible fins in the square open cavity as the time evolves from 10^{-4} to 1.375 at $E = 10^9, A = 0.1, H = 0.5$ and $t_p = 0.5$. Fig. 5(a) shows the initial state of the streamlines, and it is apparent that the fluid moves in low speed with the negative velocity values which indicate the rotation of the fluid flow at the left wall in the clockwise direction. The right wall with the opening is cooler and elucidated by the absence of the streamlines around that region. At this stage, the fluid accumulate at the left wall and evident by the small stream function contour cells. Moreover, the two identical fins retain their positions, which are orthogonal to the left heated wall. Although the flexible fins are absorbing the energy from the heated left wall, the oscillation did not occur because of the fins' characteristic as a hyperelastic material which only reacts to an enormous strain. At the surface of the heated left wall (Fig. 5(a)), there are light-weighted (less dense) fluid which is composed with the high kinetic energy molecules, while at the region far from the left wall, there are heavy-weighted (dense) fluid with low kinetic

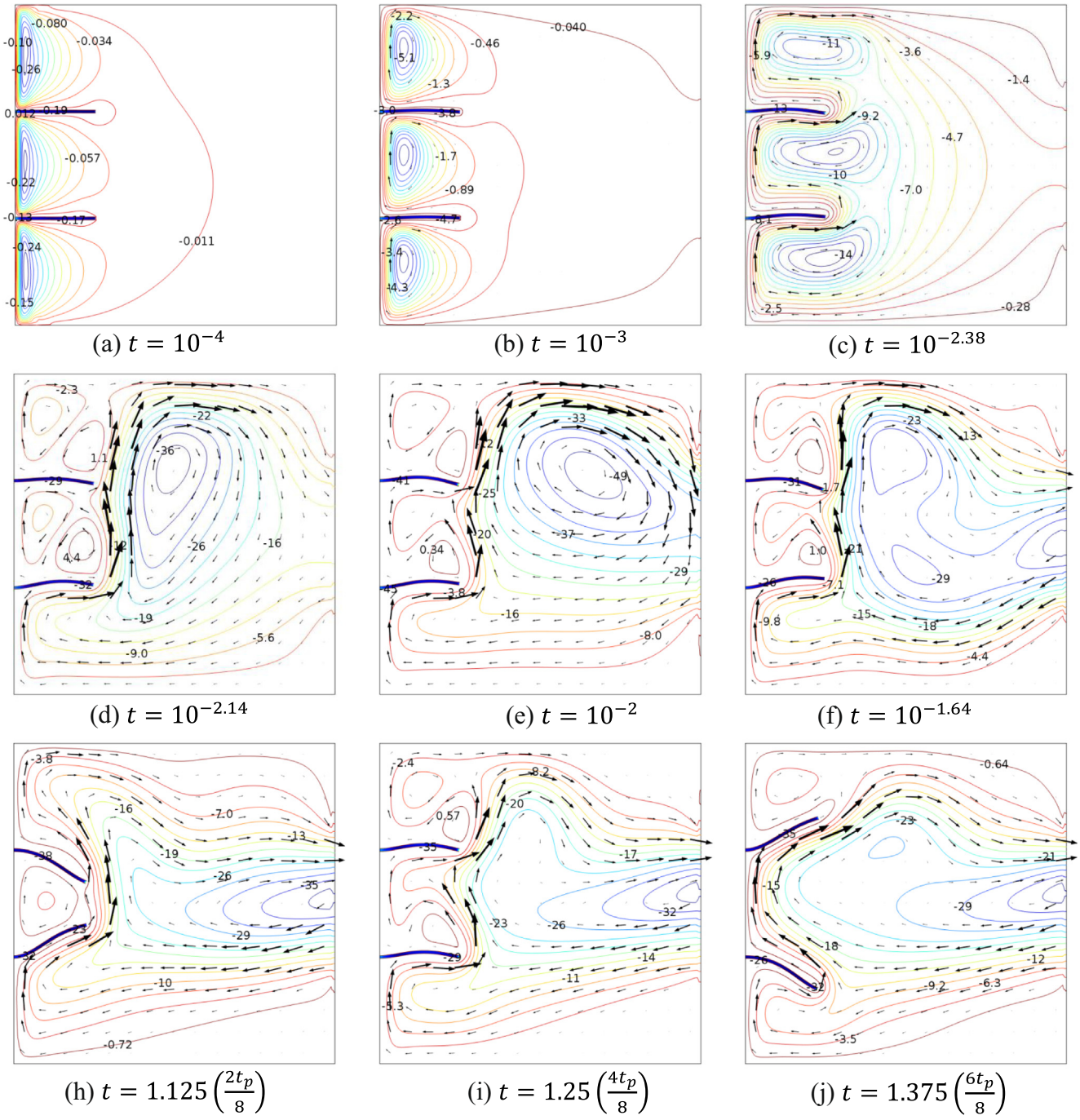

Fig. 5 Time evolution of the streamlines and velocity vectors at $L = 0.25, E = 10^9, A = 0.1, H = 0.5, Ra = 10^6$ and $t_p = 0.5$.

energy molecules. Since the driving force for natural convection is gravity, the gravity pulls the denser layer, and the fluid flow direction falls while the hotter less dense fluid rises to occupy its position. Eventually, a circulating flow is formed, and the convection process develops. These explain the rotation of the fluid flow at the left wall in the clockwise direction. Fig. 5(a) also exhibits the three inner cells which are situated at the top, middle and bottom (near the heated left wall) of the flexible fins with sharp edges. As time goes by (see Fig. 5(b)), the fluid flow towards the opening of the cavity at the right wall. This instance is because there is more dense fluid at the right wall and the less dense fluid finds the way to replace the positions of the more cooling fluids. It is also essentially a natural convection process, and the process is getting stronger. The sizes of the stream function contour cells increase, the inner cells become more substantial, and the velocity increases. The flexible fins begin to oscillate in Fig. 5b) and and probably the flexible fins have acquired enough amount of strain to commence the oscillation. The state of fins in Fig. 5(c) which are slightly bent ease the convection process from the left wall to the right wall, and it is obvious that the three different centering stream function contours from the left wall expand and

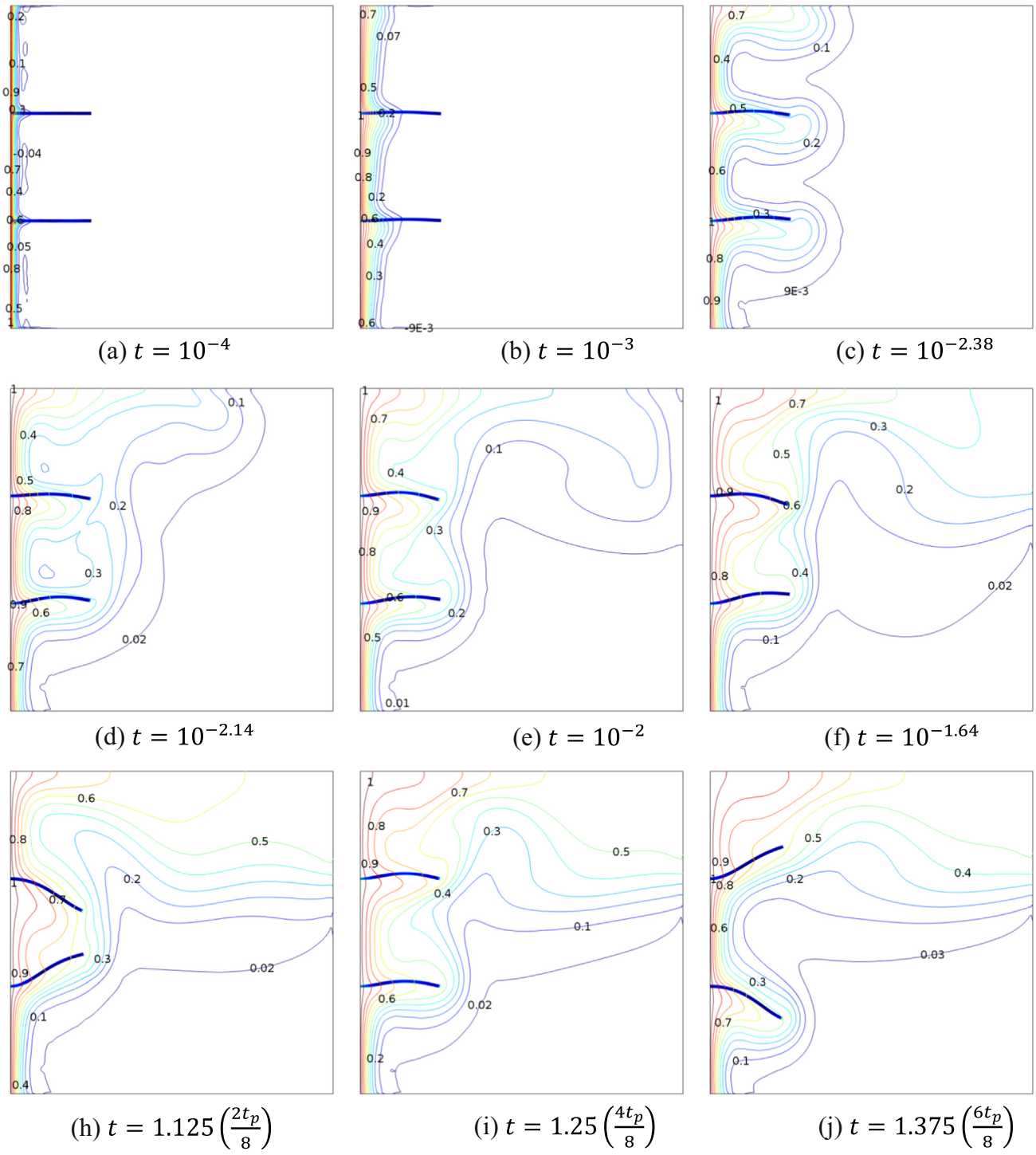

Fig. 6 Time evolution of the isotherms at $L = 0.25, E = 10^9, A = 0.1, H = 0.5, Ra = 10^6$ and $t_p = 0.5$.

move to the centre of the square cavity. Figs. 5(d)-(e) observe the progression of the stream function contours when the value of t increases from $10^{-2.14}$ to 10^{-2}, and the stream function contours with one centre take the position at the middle of the square cavity, while new stream function contours appear at the top and middle of the left wall area near the fins. The size of the contour cells are large, and the velocity is high, which clarify the presence of less dense fluid at the left wall. Further, as time increases, there is an active fluid flow at the right wall opening, and this is shown in Figs. 5(f)-(j). The velocity vectors in Fig. 5 visualize to the magnitude and directions of the mixed convection flows. The fluid speed in the velocity vectors is equivalent to the stream functions values. The vector direction indicates fluid flow motion at the time from the hot wall to the opening boundary.

Fig. 6 reports the isotherm for the same set of governing parameters' values used in previous figure as time develops. Figs. 6(a)-(b) view the hot fluid originated from the left heated

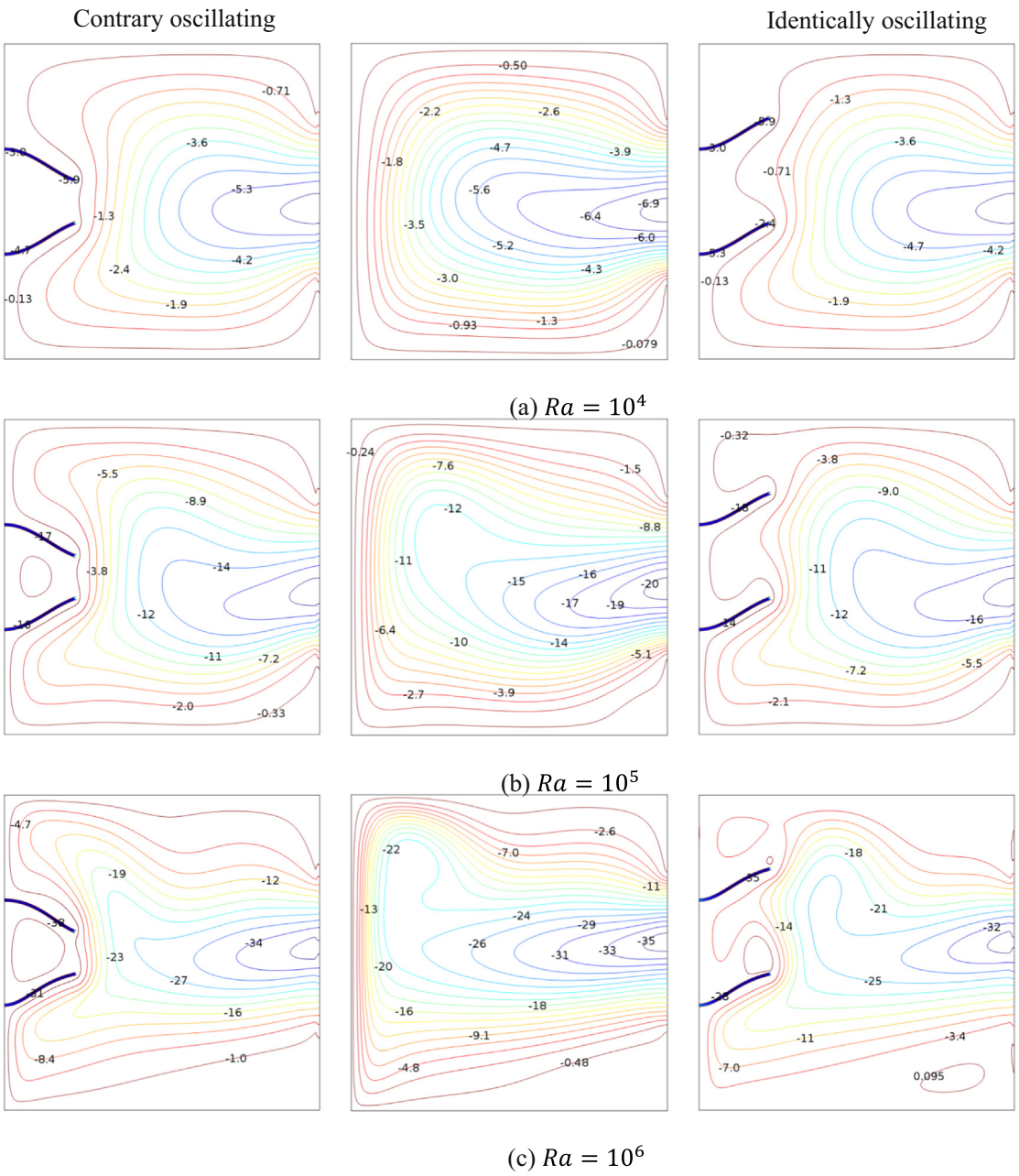

Fig. 7 Influence of the fins direction on streamlines for various Ra at $L = 0.25, E = 10^9, t_p = 0.5, A = 0.1, H = 0.5$ and $t = 1.125$.

wall and due to the significant temperature gradient between two different medium, the heat transferred conductively. This occurrence is supported by the weak isotherm contours cells that appear in between the upper wall, flexible fins and the lower wall in Fig. 6(a) which then progressively disappear in Fig. 6(b). The heat energy is transferred horizontally directed by the flexible fins' position. Isotherms in Fig. 6(c) illustrates that the natural convection begins to dominate the heat transfer process, and the heat transferred convectively heading to the middle of the cavity. The thermal boundary layer thickness gradually decreases from the left wall to the middle of the square cavity. However, the isotherm patterns from Figs. 6(-d)-(f) expose heat travel towards the opening at the right wall without traverse much at the bottom wall. The absences of the isotherm pattern at the bottom region of the cavity explain that fluid is still cold, and there is a thermal resistance at that area. The characteristic of the bottom wall, which is adiabatic resist the heat flow at the region farther from the hot left wall. In contrast, the top area of the cavity identifies an active heat transfer and proposes the less dense fluid with a higher temperature conquer the respective region. Although the upper wall is also adiabatic, yet at $Ra = 10^6$, the flow is mainly buoyancy-driven and thus urge the convective heat transfer towards the top of the cavity. Based on Figs. 6(h)-(j), the natural convection process develops well as time increases from $t = 1.125$ to $t = 1.375$, and the bottom area is essentially isothermal.

Fig. 7 inspects the streamlines pattern when the fins oscillate contrarily and identically, respectively, as Ra increases

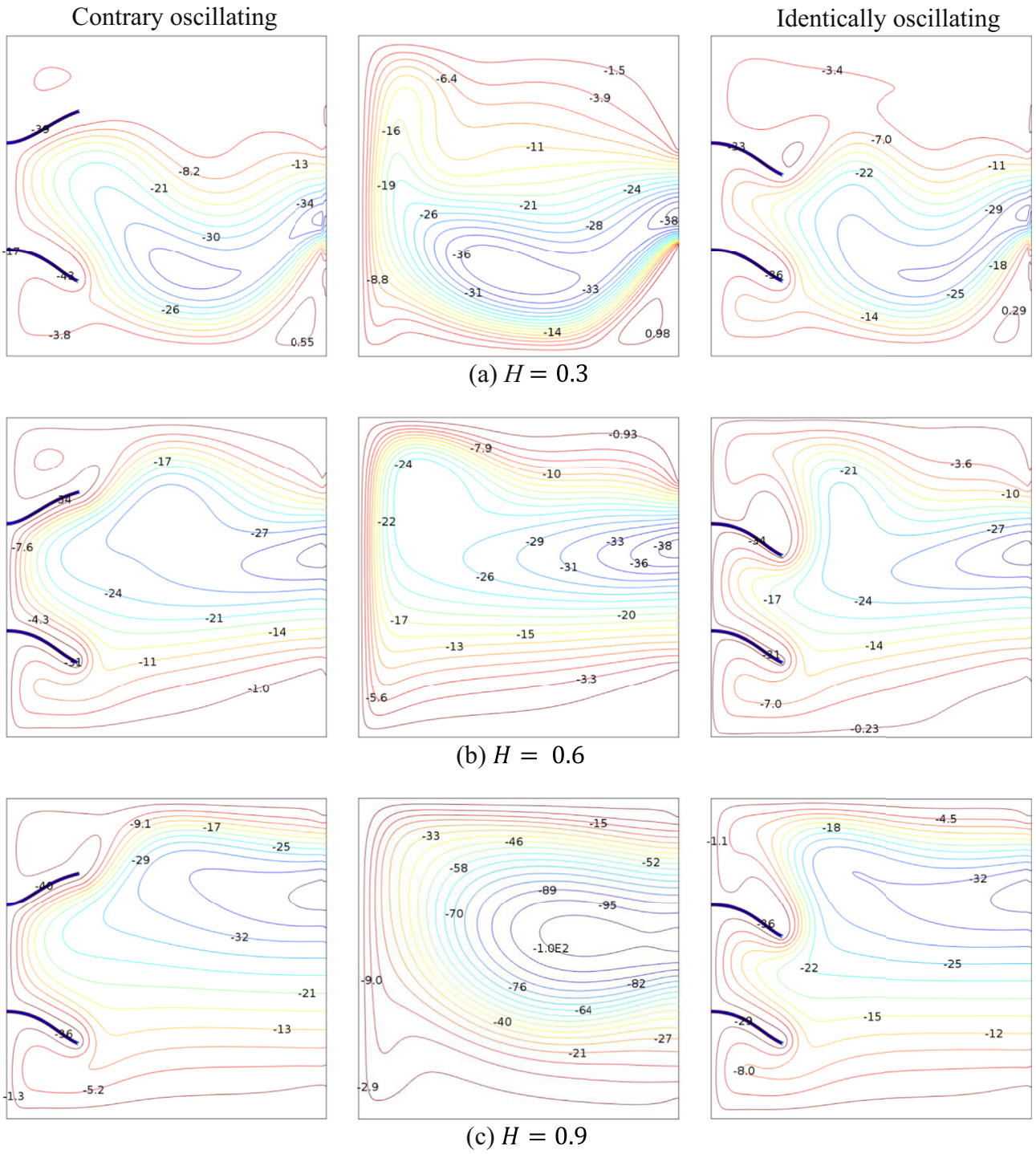

Fig. 8 Influence of the fins direction on streamlines for various H at $L = 0.25, E = 10^9, t_p = 0.5, A = 0.1, Ra = 10^6$ and $t = 1.375$.

from 10^4 to 10^6. The term "contrary oscillation" which has been introduced in the present work connotes the state of fins' oscillation in the opposite direction while "identical oscillation" signifies the fins' oscillation in the same direction. The streamlines without the presences of the oscillating fins are projected in the middle of Fig. 7, so that a clear difference can be observed. Fig. 7(a) illuminates the state of the streamlines when $Ra = 10^4$ at $t = 1.125$, where the space within the square cavity had attained a good fluid circulation towards the opening at the right wall. When the flexible fins oscillate contrarily as in Fig. 7(a), the fluid flow is absent in between of the fins because the position of the fins restrict the formation of new streamlines at a low value of Ra which expounds poor convection process, and lead the fluid towards the opening at the right wall. On the other hand, the locus of the identical oscillating fins in Fig. 7(a) allows some flow to enter the space in between the fins. Similarly, the streamlines without the oscillating fins shown in Fig. 7a) and imply a balanced fluid flow

with a low scale of velocities. The fluid flow fully occupies the square cavity, unlike the cavity, which is installed with the oscillating fins, but the flow is active at the middle of the cavity. Next, Fig. 7(b) demonstrates the streamlines of the fluid flow in the square cavity when $Ra = 10^5$. The increment in Ra shows a significant enhancement in the fluid velocity, which speeds the fluid circulation. The streamlines of the contrary and identical oscillating fins disclose the improvement in the fluid flow as there is a formation of a cell circulation in the middle of two flexible fins. Fig. 7(c) communicates the streamlines pattern influenced by the contrary and identical oscillating fins when the value of Ra increased to 10^6. The increment in Ra enriches the buoyancy effect in which induces excellent fluid flow. The stream function contour cell in between the contrary oscillating fins had expanded in size compared to the cell size when $Ra = 10^5$ and it influence the flexible fins to bent more sharper. In the streamlines pattern for the identical oscillating fins (see Fig. 7(c)), there are some newly formed stream function contours near the tip of the flexible fins and at the right bottom which infers better fluid circulation in the cavity.

Fig. 8 shows the effect of cavity opening-size (H) on the streamlines for two cases of contrary oscillating fins and identically oscillation fins. The case with no-fin is also depicted as a reference. When the fins are oscillating in a contrary manner, they act like a peristaltic pump. In this time step, the fins are diverging, which tends to intake the fluid from the opening. The flow circulation at the up and bottom regions of the cavity is almost suppressed, and the circulation is mainly at the center of the cavity. As this stage is an intake stage for this oscillation configuration, the maximum magnitude of the streamlines in the presence of fins is smaller than the case with no fins. A cavity with a larger opening provides more uniform velocities in the central regions of the cavity regardless of the presence or absence of oscillating fins.

In the case of identically oscillating fins, the oscillation behavior of the fins helps with the flow intake from the opening by a sweeping mechanism. In this case, the streamlines at the bottom of the cavity are stronger since the direction of the sweep is toward the bottom of the cavity. There is a weak circulation at the top of the cavity which can contribute to the heat transfer. The strong circulation at the bottom is more evident when the opening size is small. A small opening size can provide a good intake flow for the bottom of the cavity, but it fails to provide a good flow circulation for the top part of the cavity. The increase of the opening size improves the situation and for a large cavity size, both the top and bottom of the cavity can receive a good intake flow from the opening. In the case of identical oscillation of fins, generally, the circulation at the center of the cavity is weaker than the case of contrary oscillation of the fins. This is because there is a smaller space between the identical sweeping fins and the distribution of the fluid is smoother than the case of contrary oscillation of fins.

Fig. 9 shows the time history of the average Nusselt number for the two cases of identical and contrary oscillating fins and different Young's modules. As seen, the case of contrary oscillating provides larger maximum values of Nusselt number. Moreover, in the case of identical oscillation, the average Nusselt number is a minimum in half of the cycles. Indeed, in the case of contrary oscillation of the fins, they intake the fluid in a part of a cycle and then blow the fluid in another part of the cycle. Considering the contrary oscillating of the fins at the in the intake part of the cycle, discussed in Fig. 8 ($t = 1.375$), the Nusselt number is maximum as it sucks the fresh fluid with low temperature from the opening toward the fins and hot surface. The intake part if the cycle is when the fins are getting far

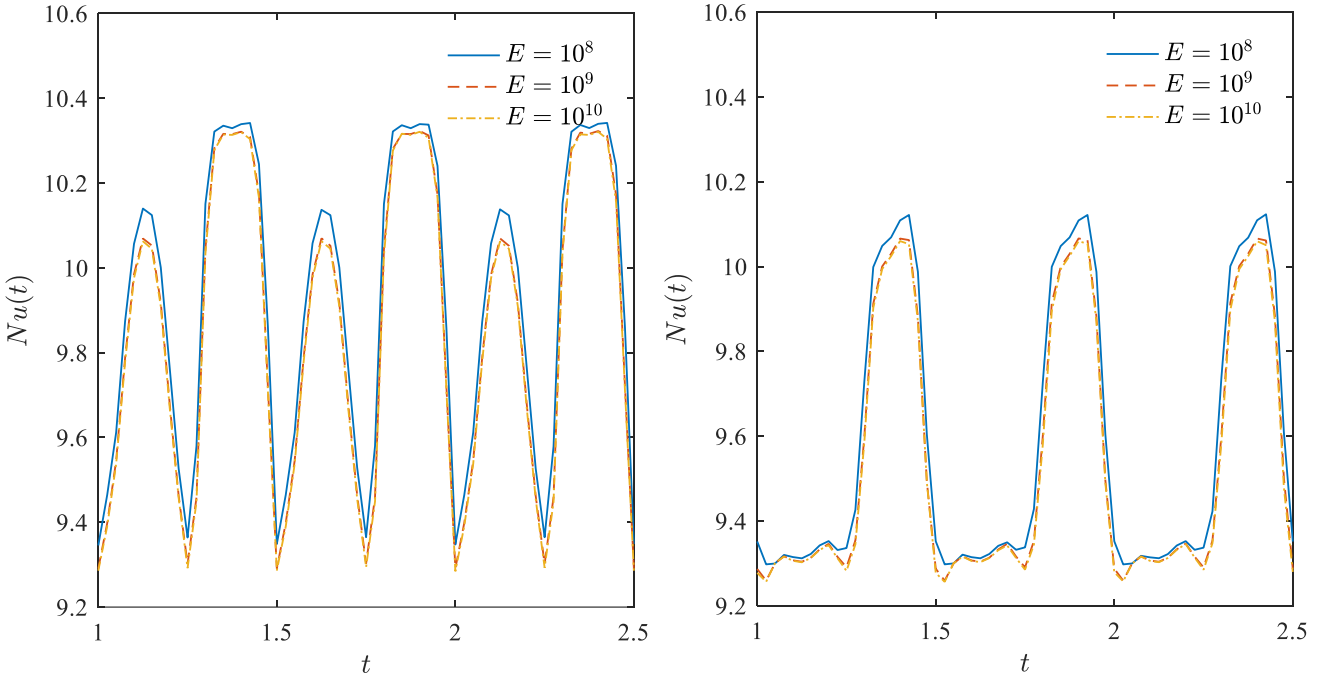

Fig. 9 Influence of the Young's modulus on the instantaneous Nusselt number for the contrary (left) and identical (right) oscillating at $L = 0.25, A = 0.1, t_p = 0.1, H = 0.5$ and $Ra = 10^6$.

from each other. When the fins are approaching each other is the blowing part of the cycle. In this case, the hot fluid next to the fins is pushing toward the outlet, and the fresh fluid can reach the fins from the top and bottom part of the cavity. As this part of the cycle involves the fresh cold water from the top and bottom sections of the cavity with limited access to fresh fluid (due to the small size of the opening, $H = 0.5$), the Nusselt number is slightly smaller than the intake part of the cycle.

In the case of identical oscillation of the fins, there is a half cycle with a low value of Nusselt number about 9.3. This is when the fins try to push the flow out of the cavity, but the trapped fluid between the fins tends to stay in between the fins. As the fins move identically, the fluid between the fins has a minimum tendency to sweep away.

The increase in the flexibility of the fins, E, improves the Nusselt number in both cases of identical and contrary oscillations. However, the improvement is only notable when E is small enough to allow significant deformation of the fins due to the interaction with the fluid. For Young's module larger than 10^9, the fin is less flexible, and hence the fin-fluid interaction does not change the deformation behavior of the fin. In the case of $E = 108$, the fin's deformation is determined by the interaction with the fluid. In this case, the deformation of the fin during the fin oscillations improves the fluid circulation, and consequently, the Nusselt number improves.

The impact of the amplitude of the fin's oscillation on the Nusselt number for two cases of contrary and identical oscillations is depicted in Fig. 10. It is observed that heat transfer is improved as the oscillation amplitude increases. A larger oscillation amplitude leads to a larger fluid circulation, which promotes heat transfer. Interestingly, when the oscillation amplitudes are too small, e.g. $A = 0.01$, the contrary and identical oscillation behaviors show almost the same range of Nusselt number. However, a slight increase of oscillation amplitude, e.g. $A = 0.03$, notably improves the Nusselt number for the case of contrary oscillation. When the oscillation amplitudes are small, the heat transfer is dominated by the natural convection heat transfer, and the little interference of the fin's motion cannot change the flow circulation and heat transfer behavior of the cavity. However, by the raise of the oscillation amplitudes, the mixed convection patterns get significant and contribute to the flow circulation and heat transfer in the cavity.

Fig. 11 displays the impact of the size of the cavity opening in the Nusselt number for two cases of contrary and identical fin oscillations. As a general behavior, the increase of the cavity opening size improves the heat transfer. There is a critical size of cavity-opening for the improvement of the heat transfer. When the cavity-opening is too small, e.g. $H = 0.3$, the Nusselt number is low. An increase in the opening size to $H = 0.6$ notably improves the Nusselt number. Further increase of the opening size, only slightly improves the heat transfer. This behavior can be justified by attention to the flow circulation nature of the cavity. The hot fluid next to the hot wall and fins tend to move upward and reach the insulated top wall. Then, the hot fluid moves along the top wall until it reaches the right upper corner of the cavity. At this stage, it tends to stay at the upper regions of the cavity. However, the cold fluid on the opening tends to move downward toward the bottom of the cavity and reaches to the hot wall. Hence, the hot fluid traped at the top of the cavity will be smoothly pushed to move downward and reach the cavity-opening. The increase in the size of the opening facilitates the escape of the hot fluid from the top regions of the cavity. The flow patterns for different cavity sizes can be seen in Fig. 8. A cavity

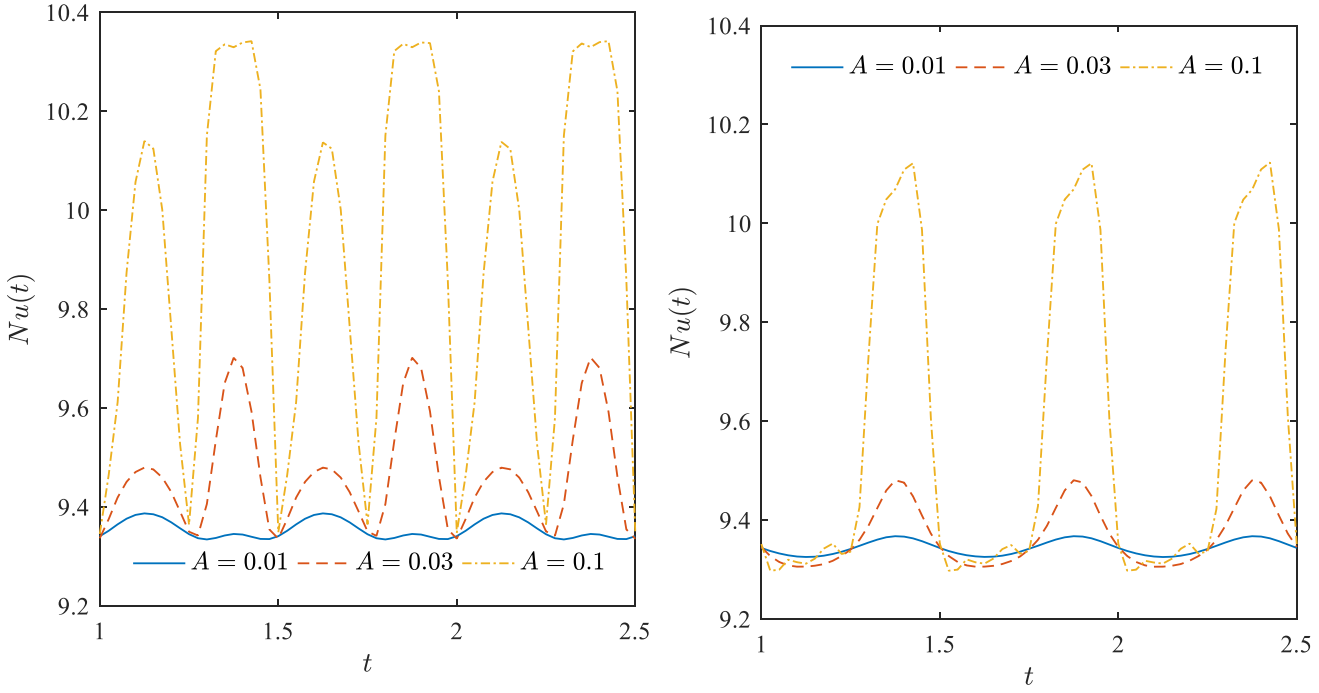

Fig. 10 Effect of the amplitude on the instantaneous Nusselt number for the contrary (left) and identical (right) oscillating at $L = 0.25, H = 0.5, t_p = 0.1, E = 10^9$ and $Ra = 10^6$.

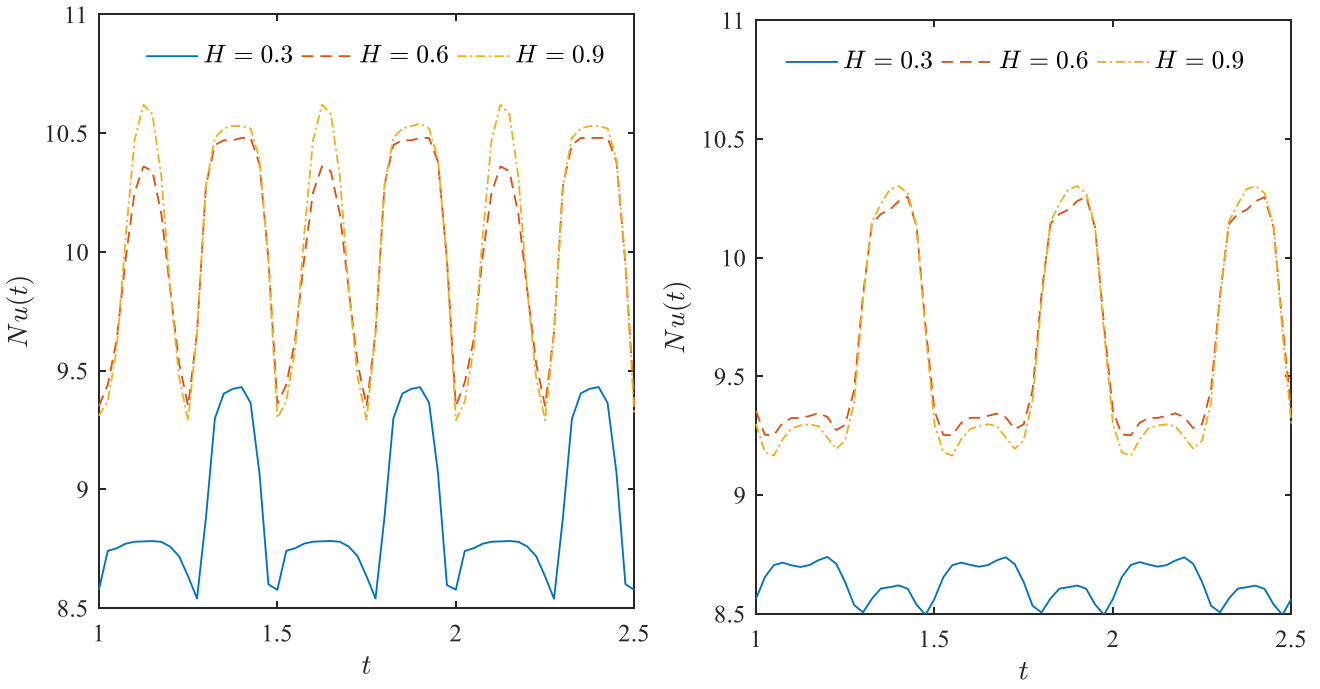

Fig. 11 Effect of the aperture size on the instantaneous Nusselt number for the contrary (left) and identical (right) oscillating at $L = 0.25, A = 0.1, t_p = 0.1, E = 10^9$ and $Ra = 10^6$.

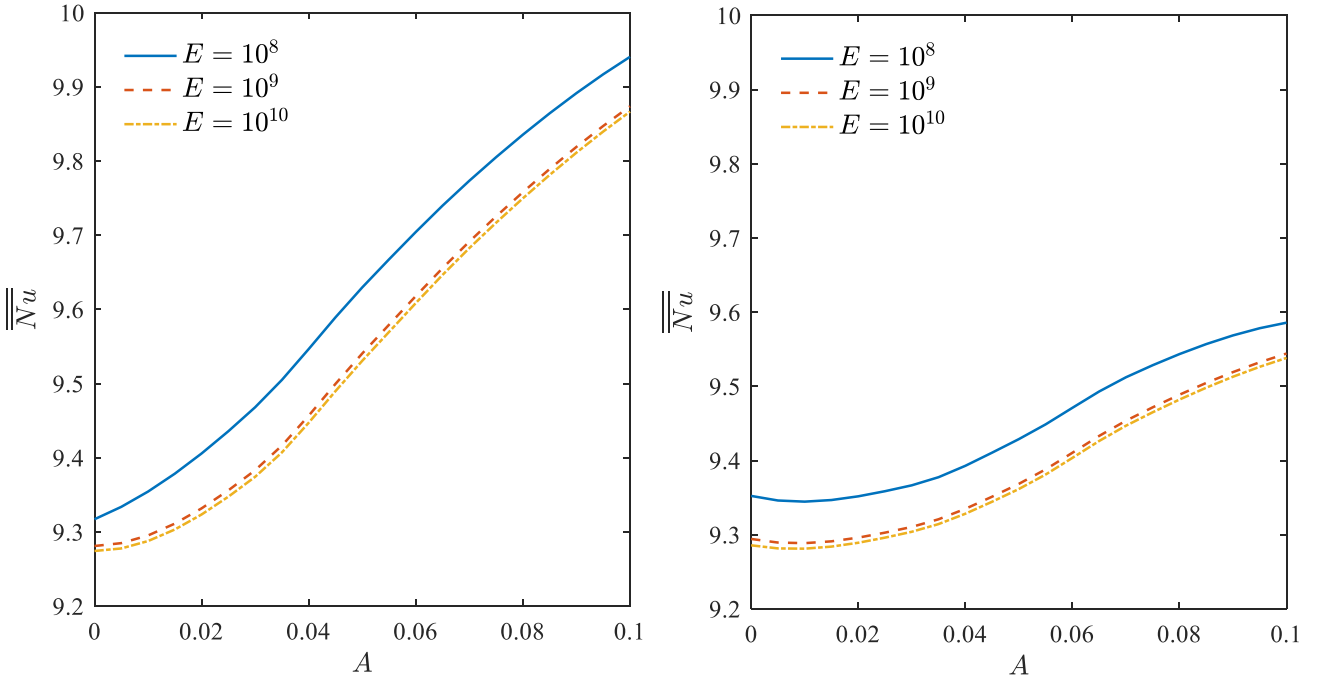

Fig. 12 Influence of the Young's modulus on the average Nusselt number with the amplitude for the contrary (left) and identical (right) oscillating at $L = 0.25, t_p = 0.1, H = 0.5$ and $Ra = 10^6$.

opening-size, which easily allows the scape of the hot fluid, can be considered as an adequate opening-size. Further increase of the cavity size only slightly contributes to the heat transfer improvement as already the trapped hot fluid is escaped.

Considering the cases of oscillating fins, the increase of the size of the cavity-opening, H, beyond the critical size, i.e. growing the opening size from $H = 0.6$ to $H = 0.9$, improves the maximum magnitude of the Nusselt number. However, it also

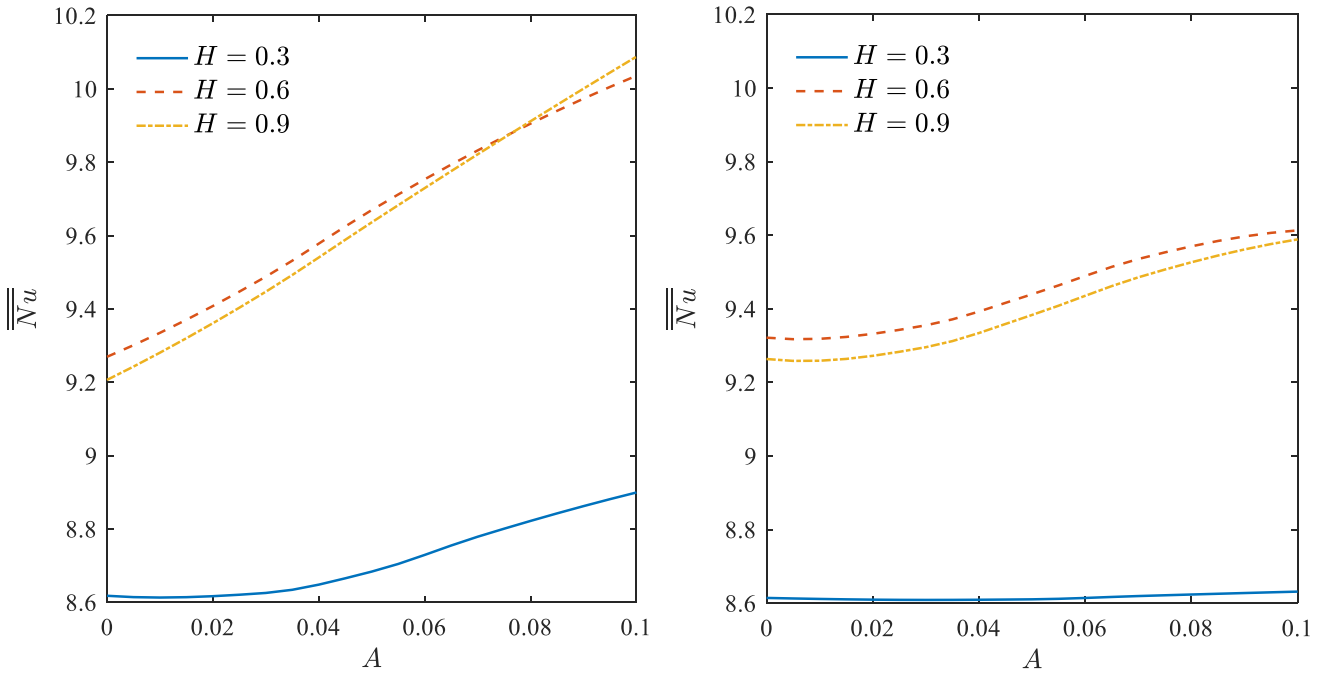

Fig. 13 Influence of the aperture size on the average Nusselt number with the amplitude for the contrary (left) and identical (right) oscillating at $L = 0.25, t_p = 0.1, E = 10^9$ and $Ra = 10^6$.

reduces the minimum value of the Nusselt number for both contrary and identical oscillating cases. The time-duration of the minimum Nusselt number, for the contrary oscillating case, is much shorter than that of the identical oscillating case. Hence, it can be concluded that the increase of the opening-size could improve the Nusselt number in the case of contrary oscillating while it reduces the Nusselt number in the case of identical oscillating.

In Figs. 12 and 13 we plot the overall Nusselt number (time-averaged Nusselt number) against the oscillation amplitude for various values of E and H, and two cases of contrary and identical oscillating fins. The results show that an increase in the flexibility of the fins (decrease of E), always promotes the overall heat transfer. A notably flexible fin yields improvement in heat transfer due to significant influence of fluid–structure interaction. Moreover, the rise of the oscillation amplitude always improves the total heat transfer. These outcomes are in good agreement with the results of Figs. 9 and 10.

Fig. 13, in agreement with the results of Fig. 11, shows that the increase of cavity-opening improves the heat transfer when the cavity opening-size is small (from $H = 0.3$ to $H = 0.6$). However, when the cavity size is adequate, $H = 0.6$, a further increase of the opening-size does not always improve the heat transfer. The reasons for possible reduction or improvement of heat transfer by the increase in the size of the cavity-opening were discussed in Fig. 11 for the time history of the Nusselt number ($Nu(t)$). As seen, in Fig. 13, the increase of H, reduces the total Nusselt number for identical oscillating behavior of fins. The same behavior can be seen for the contrary oscillating of fins, except for the case of large oscillation magnitudes. In the case of large values of A, the increase of the oscillation magnitudes changes the flow patterns during the intake and blowing portions of oscillations. Increasing the size of the cavity-opening will contribute to the intake and blowing process, which eventually improves the total heat transfer.

It is also interesting that when the size of the cavity-opening is small, $H = 0.3$, the increase of the oscillation magnitude provides a minimal impact on the overall Nusselt number in the case of identical oscillation of the fins. In this case, the identical oscillation of the fins, as discussed in Fig. 8, tends to push the fluid toward the bottom and the top of the cavity, which are the insulated section of the cavity and the cold and hot fluids will remain trapped inside the cavity. Hence, the increase of the oscillation amplitude just increases the magnitude of the fluid velocity toward the insulated sections of the cavity and does not contribute to the heat transfer. In contrast, in the case of contrary oscillating, the increase of the oscillation amplitude notably contributes to the promotion of heat transfer rate. This is due to the intake and blowing behavior of contrary oscillation fins, which helps with the escape of trapped fluids in the cavity with a small opening.

5. Conclusions

The present study scrutinized the impact of fluid (air) and structure (dual flexible oscillating fins) interaction towards the natural convection mechanism in a square open cavity. The finite element Galerkin method with the aid of the ALE procedure were utilised to solve the mathematical model. The results were organized in terms of the streamlines, isotherms, instantaneous and average heat transfer characteristics. The outcome of the present numerical solutions are summarized as follows:

1. An increment in the Rayleigh number improves the fluid velocity and forms stronger fluid circulation. The contrary fins oscillation yields better fluid circulation than the fins which oscillate identically.

2. The increment in the aperture size enhances the strength of the fluid circulation, and the identical oscillating fins permit better fluid circulation at the hot left wall.
3. The increment in the aperture size gives a significant local heat transfer improvement while a small-amplitude oscillation maintains a low instantaneous Nusselt number.
4. A maximum heat transfer enhancement happens at the suitable parameters between the aperture size and the fins oscillating direction. Moreover, heat transfer enhancements reach to a maximum point at the extreme amplitude tip configuration for the high flexibility.

These results can be applied in configuring vent openings of the computer processing devices to help ensure optimal and safe working conditions.

Declaration of Competing Interest

The authors declare that they have no known competing financial interests or personal relationships that could have appeared to influence the work reported in this paper.

Acknowledgment

The work was supported by the Malaysian Ministry of Education research grant FRGS/1/2019/STG06/UKM/01/2.

References

[1] S. Gupta, D. Kumar, J. Singh, MHD mixed convective stagnation point flow and heat transfer of an incompressible nanofluid over an inclined stretching sheet with chemical reaction and radiation, Int. J. Heat Mass Transf. 118 (2018) 378–387.
[2] S. Gupta, D. Kumar, J. Singh, S. Gupta, Impact of generalized Fourier's law and Fick's law for MHD flow of Ag-H_2O and TiO_2-H_2O nanomaterials, Multidiscip. Model. Mater. Struct. 15 (2019) 1075–1099.
[3] S. Gupta, D. Kumar, J. Singh, Magnetohydrodynamic three-dimensional boundary layer flow and heat transfer of water-driven copper and alumina nanoparticles induced by convective conditions, Int. J. Mod. Phys. B 33 (2019) 1950307.
[4] S. Ostrach, Natural convection in enclosures, Adv. Heat Transf. 8 (1972) 161–227.
[5] G. de Vahl Davis, Natural convection of air in a square cavity: A benchmark numerical solution, Int. J. Numer. Meth. Fluids 3 (1983) 249–264.
[6] S. Ostrach, Natural convection in enclosures, J. Heat Transf. 110 (1988) 1175–1190.
[7] F. Penot, Numerical calculation of two-dimensional natural convection in isothermal open cavities, Numer. Heat Transf. Part A 5 (1982) 421–437.
[8] Y.L. Chan, C.L. Tien, A numerical study of two-dimensional natural convection in square open cavities, Numer. Heat Transf. Part A 8 (1985) 65–80.
[9] A. Abib, Y. Jaluria, Numerical simulation of the buoyancy-induced flow in a partially open enclosure, Numer. Heat Transf. Part A 14 (1988) 235–254.
[10] D. Angirasa, M.J. Pourquie, F. Nieuwstandt, A numerical study of steady and transient laminar buoyancy driven flow and heat transfer in a square open cavity, Numer. Heat Transf. Part A 22 (1992) 223–239.
[11] D. Angirasa, J.G.M. Eggels, F.T.M. Nieuwstandt, Numerical simulation of transient natural convection from an isothermal cavity open on a side, J. Fluid Mech. 28 (1995) 755–768.
[12] W. Chakroun, M. Elsayed, S. Al-Fahed, Experimental measurements of heat transfer coefficient in a partially/fully opened tilted cavity, J. Sol. Eng. 119 (1997) 298–303.
[13] M. Elsayed, N. Al-Najem, M. El-Refaee, A. Noor, Numerical study of natural convection in fully open tilted cavities, Heat Transf. Eng. 20 (1999) 73–85.
[14] E. Bilgen, H. Oztop, Natural convection heat transfer in partially open inclined square cavity, Int. J. Heat Mass Transf. 48 (2005) 1470–1479.
[15] G. Lauriat, G. Desrayaud, Effect of surface radiation on conjugate natural convection in partially open enclosures, Int. J. Thermal Sci. 45 (2006) 335–346.
[16] N. Kasayapanand, Numerical modeling of natural convection in partially open square cavities under electric field, Int. Comm. Heat Mass Transf. 34 (2007) 630–643.
[17] N. Kasayapanand, Enhanced heat transfer in partially open square cavities with thin fin by using electric field, Energy Convers. Manag. 50 (2009) 287–296.
[18] A. Mahmoudi, M. Shahi, A. Shahedin, N. Hemati, Numerical modeling of natural convection in an open cavity with two vertical thin heat sources subjected to a nanofluid, Int. Comm. Heat Mass Transf. 38 (2011) 110–118.
[19] G. Kefayati, S. Hosseinizadeh, M. Gorji, H. Sajjadi, Lattice Boltzmann simulation of natural convection in an open enclosure subjugated to water/copper nanofluid, Int. J. Thermal Sci. 52 (2012) 91–101.
[20] J. Wang, Y. Zhou, Q. Deng, Buoyancy-induced flow and heat transfer in multilayered cavities with openings, Int. J. Numer. Meth. Heat Fluid Flow 28 (2018) 1774–1790.
[21] W. Sheu, G. Chen, C. Wang, Performance of piezoelectric fins for heat dissipation, Int. J. Heat Mass Transf. 86 (2015) 72–77.
[22] A. Soti, R. Bhardwaj, J. Sheridan, Flow-induced deformation of a flexible thin structure as manifestation of heat transfer enhancement, Int. J. Heat Mass Transf. 84 (2015) 1070–1081.
[23] S. Ali, S. Menanteau, C. Habchi, T. Lemenand, J. Harion, Heat transfer and mixing enhancement by using multiple freely oscillating flexible vortex generators, Appl. Thermal Eng. 105 (2016) 276–289.
[24] M. Ghalambaz, E. Jamesahar, M. Ismael, A. Chamkha, Fluid-structure interaction study of natural convection heat transfer over a flexible oscillating fin in a square cavity, Int. J. Thermal Sci. 111 (2017) 256–273.
[25] A. Alsabery, M. Sheremet, M. Ghalambaz, A. Chamkha, I. Hashim, Fluid-structure interaction in natural convection heat transfer in an oblique cavity with a flexible oscillating fin and partial heating, Appl. Thermal Eng. 145 (2018) 80–97.
[26] H. Saleh, Z. Siri, I. Hashim, Role of fluid-structure interaction in mixed convection from a circular cylinder in a square enclosure with double flexible oscillating fins, Int. J. Mech. Sci. 161–162 (2019) 105080.
[27] S. Mehryan, A. Alsabery, A. Modir, E. Izadpanahi, M. Ghalambaz, Fluid-structure interaction of a hot flexible thin plate inside an enclosure, Int. J. Thermal Sci. 153 (2020) 106340.
[28] M. Ghalambaz, S. Mehryan, R. Feeoj, A. Hajjar, I. Hashim, R. Mahani, Free convective heat transfer of a non-Newtonian fluid in a cavity containing a thin flexible heater plate: an Eulerian-Lagrangian approach, J. Therm. Anal. Calorim. (2020) 1–16, https://doi.org/10.1007/s10973-020-10292-y, In press.
[29] E. Jamesahar, M. Sabour, M. Shahabadi, S. Mehryan, M. Ghalambaz, Mixed convection heat transfer by nanofluids in a cavity with two oscillating flexible fins: A fluid–structure interaction approach, Appl. Mathl. Model. 82 (2020) 72–90.

[30] M. Ismael, H. Jasim, Role of the fluid-structure interaction in mixed convection in a vented cavity, Int. J. Mech. Sci. 135 (2018) 190–202.

[31] Y. Bazilevs, K. Takizawa, T.E. Tezduyar, Computational fluid-structure interaction: methods and applications, John Wiley & Sons, 2013.

[32] J. Hinojosa, R. Cabannilas, G. Alvarez, C. Estrada, Nusselt number for the natural convection and surface thermal radiation in a square tilted open cavity, Int. Commun. Heat Mass Transf. 32 (2005) 1184–1192.